Pis'ma v ZhETF, vol. 93, iss. 2, pp. 73 – 77

Evidence for strong Coulomb correlations in metallic phase of vanadium dioxide

A. S. Belozerov°, *A. I. Poteryaev**°[1], *V. I. Anisimov*°

°*Institute of Metal Physics, Russian Academy of Sciences, 620041, Ekaterinburg GSP-170, Russia*

**Ural Federal University, 620002 Ekaterinburg, Russia*

Submitted 29 November 2010

The influence of Coulomb correlation on magnetic and spectral properties in metallic rutile phase of vanadium dioxide is studied by state of the art LDA+DMFT method. Calculation results in strongly correlated metallic state with an effective mass renormalization $m^*/m \approx 2$. Uniform magnetic susceptibility shows Curie-Weiss temperature dependence with effective magnetic moment, $p_{\text{eff}}^{\text{theor}} = 1.54\mu_B$, in a good agreement with the experimental value $p_{\text{eff}}^{\text{exp}} = 1.53\mu_B$ that is close to ideal value for V^{4+} ion with the spin $S = 1/2$, $p_{eff} = 1.73\mu_B$. Calculated spectral function shows well developed Hubbard bands observable in the recent experimental photoemission spectra. We conclude that VO_2 in rutile phase is strongly correlated metal with local magnetic moments formed by vanadium *d*-electrons.

Transition metal compounds and particularly vanadium oxides attract a lot of interests because of rich variety of structural modifications and properties [1]. Vanadium dioxide is not an exception and is well known due to metal-insulator transition at 340 K [2]. The value of the energy gap (Δ_g=0.6 eV) in insulating phase and vicinity of the transition and room temperatures allows one to use this material as "wisdom" windows and in another termochromic applications [3]. This compound has been extensively investigated experimentally and theoretically over the half of century. The phase diagram [2] in the temperature-pressure (or chemical doping) coordinates consists of the paramagnetic metal at high temperature and three insulating states below T_c. Above the transition temperature VO_2 crystallizes to rutile structure at all values of doping (see Fig.1). Below transition temperature there are three insulating phases, called M_1, T and M_2 at low, intermediate and large values of doping, respectively. In these phases the conductivity drops by factor of several orders in magnitude comparing to rutile phase with the estimation of the energy gap about 0.6 eV [4].

Most of earlier theoretical studies for correlation effects in vanadium dioxide were concentrated on the insulating low-temperature phases where band structure calculations have difficulties to reproduce correct insulating type of electronic structure [5 – 7]. Calculation for rutile crystal structure resulted in metallic bands in agreement with experiment, and hence, it was assumed that taking into account Coulomb correlations is not needed here. However magnetic and spectral measurements for VO_2 show that correlation strength could be essential for metallic rutile phase [8, 9]. The magnetic experiments for metallic rutile phase show a quite large temperature dependent magnetic susceptibility that indicates formation of local magnetic moment in the partially filled *d*-band. Recent photoemission data [8] display the quasi-particle peak at the Fermi level and high energy structure associated with the lower Hubbard band about -1 eV. The effective electron mass, m^*/m, extracted from optics [9] is about 4.3 which is larger then the value observed for $Sr_xCa_{1-x}VO_3$ characterized as moderately correlated paramagnetic metals [10]. Recent LDA+DMFT investigations [11] of vanadium oxide have paid an attention to the spectral properties of the compound and have showed a good agreement with photoemission and optical data.

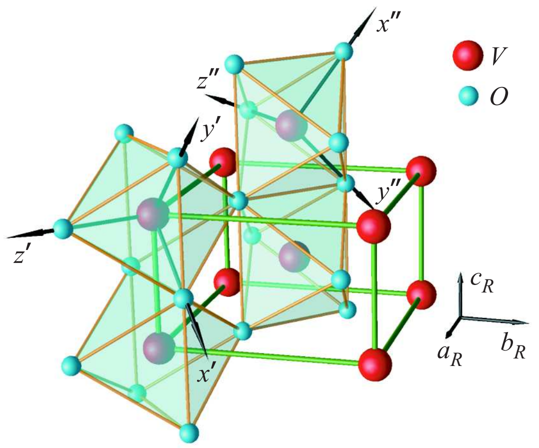

Fig.1. Crystal structure of rutile phase. Vanadium and oxygen atoms are denoted by large (red) and small (cyan) balls. (a_R, b_R, c_R) are rutile crystallographic axes and coincide with the Cartesian one. Local coordinate axes on the vanadium atoms are shown by (double) primed set

[1]e-mail: poter@optics.imp.uran.ru

In the present work we have used state of the art LDA+DMFT method [12] to study the physics of VO_2 in metallic rutile phase with the special focus on the magnetic properties. Temperature dependence of the calculated magnetic susceptibility $\chi(T)$ reproduces with a good accuracy Curie-Weiss law $\chi_{CW}(T) = p^2_{\text{eff}}/3(T-\Theta)$ and is in an agreement with experimental data. Calculations results for the spectral function are typical for strongly correlated metal with well developed Hubbard bands in addition to quasi-particle metallic peak at Fermi level and they agree well with earlier studies [11].

At high temperatures, vanadium dioxide crystallizes as rutile shown on the Fig.1. Details of lattice constants and atomic positions can be found in Ref. [13]. Each vanadium atom is surrounded by a oxygen's octahedron resulting in splitting of d level to triply degenerate t_{2g} and doubly degenerate e_g^σ states. Additional tetragonal distortion present in the structure leads to further lifting of degeneracy of t_{2g} level to a_{1g} and π states ($d_{||}$ and d_π according to Gooenough's notations [5]). In the local coordinate basis shown on the Fig.1 by (double) primed axes for vanadium atoms, a_{1g} state corresponds to the $d_{x'y'}$ orbital, π states correspond to $d_{x'z'}$ and $d_{y'z'}$ and e_g^σ to $d_{z'^2}$ and $d_{x'^2-y'^2}$ orbitals. The local z' axis is chosen to be pointed to apical oxygens and local x' and y' are chosen to be pointed to the planar one. The double primed local coordinate axes are obtained by a proper symmetry operation for corresponding vanadium atoms.

We used TB-LMTO method [14] to calculate electronic structure of VO_2. The results obtained are presented on the Fig.2 and have a good agreement with earlier studies [7]. One can clearly see that the states crossing Fermi level are of vanadium t_{2g} symmetry mainly and spread from -0.5 to 2 eV. They are well separated by a gap of 1.4 eV from occupied bonding states of mixed O $2p$ and V e_g^σ character. The anti-bonding combination is located above 2 eV and is also separated by a tiny gap from the t_{2g} bands. The orbitally (symmetry) decomposed partial DOSes for vanadium atom in the local coordinate system mentioned above are presented on the bottom panel of Fig.2. a_{1g} state is more narrow than π one and has a one-dimensional-like shape.

We constructed low-energy Hamiltonian for V t_{2g} states using the NMTO method [15]. It has a dimension of 6 and will be used in LDA+DMFT calculation. The eigenvalues of the NMTO Hamiltonian coincide with the LMTO's one by construction in the energy interval close to the Fermi level and shape of the density of states remains the same (not presented). Hopping integrals for the Wannier function of a_{1g}, π_1 and π_2 ($d_{x'y'}, d_{x'z'}$ and $d_{y'z'}$ in local notations) symmetries are presented in the Table for the vanadium atoms in chain (along c_R axis) and between chains (upper and lower parts of table, respectively). One can immediately see that a_{1g} electron can easily jump to the same orbital on the nearest neighbor atom and it is the largest (intra chain) hopping. The probability to hop to another chains is much smaller for a_{1g} electron. Overall structure of a_{1g} hoppings assumes one-dimensional-like physics where the largest transfer integral defines energy splitting between peaks and the rest is responsible for asymmetry of density of states and its broadening (see a_{1g} partial DOS on the bottom panel of Fig.2). The structure of the π hoppings is more uniform in space that produces more three dimensional shape of density of states.

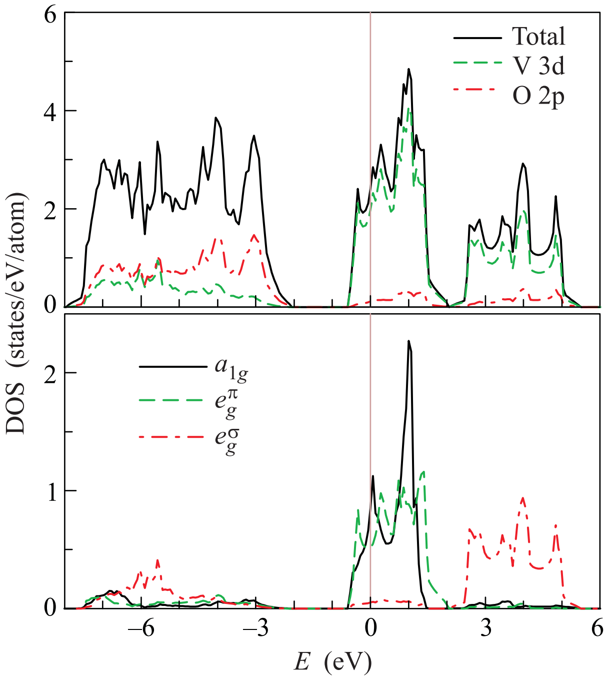

Fig.2. LDA density of states. Top panel shows total, V $3d$ and O $2p$ DOSes by (black) solid, (green) dashed and (red) dot-dashed lines, respectively. Bottom panel shows partial DOSes of different symmetry for vanadium atom (see legends for notations)

Hopping integrals for the rutile phase (in meV). The distance between vanadium atoms is in second column. The largest hoppings to another atoms are smaller than 25 meV and not shown here

	d, Å		a_{1g}	π_1	π_2
Intra chain hopping	2.85	a_{1g}	-310	0	0
		π_1	0	63	155
		π_2	0	155	63
Inter chain hopping	3.52	a_{1g}	6	0	0
		π_1	40	-177	26
		π_2	-40	-177	26

To take into account electron-electron correlation in the partially filled d-band we use LDA+DMFT method [12]. It combines the material specific aspect in LDA and accurate treatment of local Coulomb interaction in DMFT [16, 17]. The later is achieved via mapping of the lattice problem with many degrees of freedom to the quantum impurity embedded to the time dependent self-consistent bath (for details about LDA+DMFT method and implementations see e.g. Refs [18]). For the solution of the quantum impurity problem the modern multi-orbital Hirsch-Fye quantum Monte-Carlo method has been used [19]. In our LDA+DMFT calculations we use the value of screened Coulomb interaction, U=4 eV, and the value of Hund's exchange, J=0.68 eV.

We start the presentation of the LDA+DMFT results from magnetic properties. Following the linear response idea, the uniform magnetic susceptibility can be calculated directly by adding to the Hamiltonian an external magnetic field, $\mu_B H_z$, and measuring magnetization of compound. Then, the uniform magnetic susceptibility is

$$\chi(T) = m(T)/H_z, \tag{1}$$

where $m(T) = \sum_m n_m^{\uparrow} - n_m^{\downarrow}$ is a magnetization at given temperature. The few magnetic fields of order $\sim 0.02 \div 0.1$ eV were used to check and satisfy the condition of linearity of magnetization. The inverse of calculated uniform magnetic susceptibility and experimental data extracted from Ref. [20] are shown on the Fig.3. One can clearly see that these inverse quantities agree

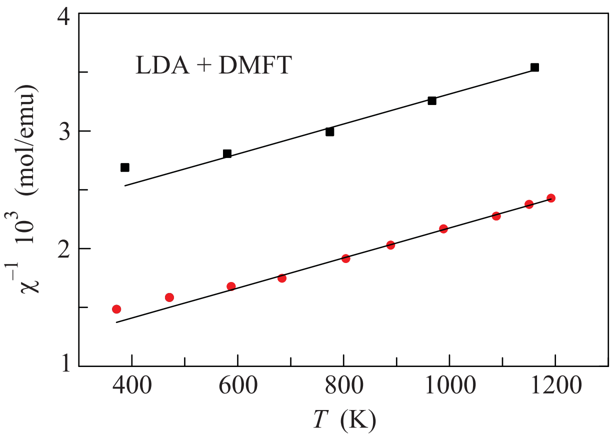

Fig.3. Inverse of uniform magnetic susceptibility. LDA+DMFT results are shown by (black) squares, the experimental data by Zylbersztejn et al. [20] are (red) circles. Lines are linear fit result

accurately to the shift along ordinate axis. This implies that the calculated and experimental effective magnetic moments are in good agreement. The theoretical estimate obtained by the fit to the Curie-Weiss law

$$\chi_{CW}(T) = p_{\text{eff}}^2/3(T-\Theta) \tag{2}$$

gives the value of the effective magnetic moment, $p_{\text{eff}}^{\text{theor}} = 1.54\mu_B$, in a good agreement with the experimental value $p_{\text{eff}}^{\text{exp}} = 1.53\mu_B$ that is close to ideal value for V^{4+} ion with the spin $S = 1/2$, $p_{\text{eff}} = 1.73\mu_B$. To make the fit shown by lines we have used the data points above 500 K where the linearity of χ^{-1} is more pronounced for theoretical and experimental data as well [21]. The theoretical Curie-Weiss temperature Θ is almost twice larger then its experimental counterpart (-1600 K and -700 K correspondingly), that is connected to the mean-field nature of the calculations and, hence, absence of the collective excitations.

We have also calculated a local spin-spin correlation function, $\langle S_z(\tau)S_z(0)\rangle$ at different temperatures shown on the Fig.4. Albeit this is a pure local quantity and

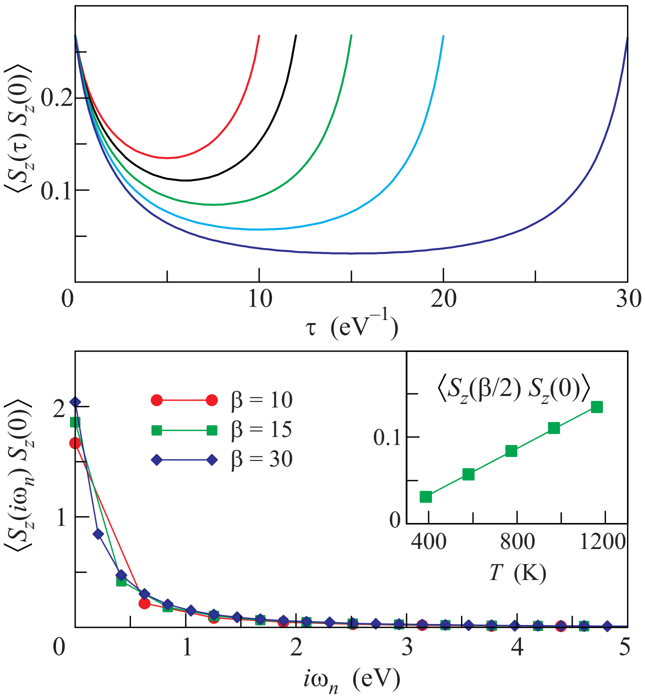

Fig.4. The local spin-spin correlation function for different temperatures in imaginary time domain (upper panel) and its Fourier transform (lower panel). Inset shows the dependence of this correlator at $\beta/2$ with temperature

cannot be directly compared to the experimental data, it gives a sound source of information about magnetic properties of the system. At low temperatures, in the Fermi liquid regime, the local spin-spin correlation function behaves as $[T/\sin(\pi\tau T)]^2$ at intermediate times, τ, while it saturates to the constant value for the insulator or metal with a very well developed local magnetic moment [17, 22]. At middle point, the correlator is $\langle S_z(\beta/2)S_z(0)\rangle \approx T^\alpha$, with exponent α=2 for Fermi liquid and zero for the insulator. On the upper panel of the Fig.4, from the time dependency one can see that the correlation function is not saturated. At the same time, the $\langle S_z(\beta/2)S_z(0)\rangle$ quantity plotted in the inset shows the linear behavior with the exponent α=1 different from both insulating and metallic regimes. This observation suggests that the formation of the local magnetic moment in the metallic phase is not completely finished [22]. The lower panel of the Fig.4 shows the Fourier transform of the local spin-spin correlation function to the Matsubara grid. The width of the peak at zero frequency is inverse proportional to a "lifetime" of the local magnetic moment and it is much larger than that of the α-iron in paramagnetic phase [23] which is closer to the localized limit.

Now, we would like to turn our discussion to single particle properties. The imaginary part of the self-energy for a_{1g} and π orbitals are shown on the Fig.5. The behavior of the imaginary part for both orbitals

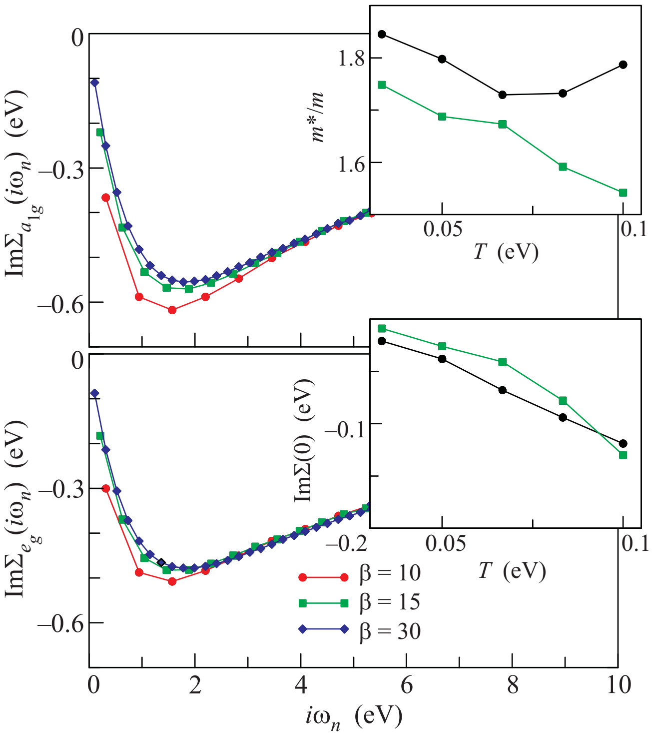

Fig.5. Imaginary part of self-energy for a_{1g} (top) and e_g (bottom) states in metallic phase. Solid (blue), dashed (green) and dot-dashed (red) lines present β=30, 15 and 10 eV^{-1} respectively (~390, 770 and 1160 K). Upper inset shows the effective mass, m^*/m, for a_{1g} and e_g orbitals by (black) circles and (dark green) squares, respectively. Lower insets shows the imaginary part of self-energy extracted to zero energy, $\Im\Sigma(0)$

is of Fermi-liquid type. At small real frequencies, in Fermi-liquid regime, the imaginary part is $\Im\Sigma(\omega) = -\Gamma T^2 - B\omega^2$ that transforms to the linear behavior on the Matsubara axis, $\Im\Sigma(i\omega_n) = -\Gamma T^2 - B\omega_n$, observable on the figure. Additionally, the mass enhancement factor

$$m^*/m = 1 - \Im\Sigma(i\omega_0)/\omega_0 \qquad (3)$$

as a function of temperature shows a saturation (upper inset of Fig.5) indicating the Fermi-liquid behavior [24] of moderately correlated metal with $m^*/m \approx$ 1.8 and 1.7 for a_{1g} and π orbitals, respectively. The lower inset shows the extracted to zero imaginary part of self-energy, $\Im\Sigma(0)$ versus temperature. One can see that it goes quadratically to zero at low temperatures once again confirming Fermi-liquid nature of compound. From these data one can conclude that the coherence temperature is about 700 K for both orbitals.

The comparison of the photoemission data [8] (PES) with the calculated LDA and LDA+DMFT results are presented on the upper panel of the Fig.6. One can

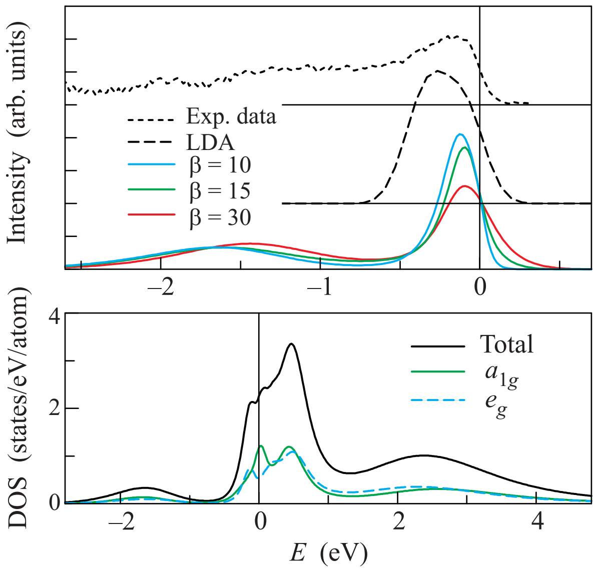

Fig.6. Top panel shows comparison of the photoemission data extracted from the Ref. [8] and calculated LDA and LDA+DMFT results for various temperatures. Bottom panel is total and orbitally resolved LDA+DMFT spectral functions for β=30 eV^{-1}

clearly observe a good agreement of the LDA+DMFT (color lines) and PES data (dots). There is a quasiparticle peak at the Fermi level and lower Hubbard band at higher energies. The later is an additional evidence of the correlated nature of the metallic rutile phase. Temperature dependence of the LDA+DMFT spectra shown by different colors is also in good qualitative agreement with the experiment (see Fig.3 of the Ref. [8]): the spectral weight is transferred from quasi-particle peak to higher energies and becomes smaller with decrease of temperature. At the same time, the LDA results shown by the dashed line describe the quasi-particle feature at the Fermi level with a large overestimation of the peak weight and complete absence of the high energy incoherent hump. LDA+DMFT spectral function for lowest calculated temperature, $T \approx 390$ K, is presented on the lower panel of the Fig.6. One can clearly see the three peaks structure which is typical for correlated materials. The quasi-particle peak lies at/above the Fermi level and low and upper Hubbard bands are located at higher frequencies, at -1.5 eV and ~ 2.3 eV. The width of the quasi-particle peak is reduced to ~ 1.1 eV comparing with 2.1 eV value for non-interacting band width and is almost independent with temperature which is compatible with the weak temperature dependence of the quasi-particle weight, $Z = m/m^*$, for both orbitals (see upper inset of Fig.5). One should note here that the spectral functions for higher temperatures are similar to described above. The difference is that the shape of the quasi-particle peak becomes more complicated due to the decrease (in absolute value) of the imaginary part of self-energy at zero energy (see lower inset of the Fig.5), and hence, displaying the features of original LDA spectral function smoothed by high temperature at β=10 eV^{-1}.

In conclusion we have studied the influence of Coulomb correlation effects on magnetic and spectral properties of VO_2 in metallic rutile phase by LDA+DMFT method. The calculation results show typical strongly correlated metal behavior for self-energy with a sizable spectral weight transfer to Hubbard bands and electronic states renormalization near the Fermi level with effective mass $m^*/m \approx 2$. The uniform and local magnetic susceptibility calculation obey Curie-Weiss temperature dependence with effective magnetic moment value close to ideal ionic value corresponding to d^1 configuration. A good agreement of calculated and measured spectral and magnetic properties allows to conclude that VO_2 in rutile phase is in strongly correlated metal state with local magnetic moments formed by d-electrons.

The authors thank A. Georges and S. Biermann who were at the initial stage of this work and A. Katanin and A. Lichtenstein for useful discussions. AP thanks to the Marie Curie grant # MIF1-CT-2006-021820. This work was supported by the Russian Foundation for Basic Research (Projects # 10-02-00046a, # 08-03-00930a), the Dynasty Foundation, the Program of the Russian Academy of Science Presidium "Quantum microphysics of condensed matter" N7.

1. M. Imada, A. Fujimori, and Y. Tokura, Rev. Mod. Phys. **70**, 1039 (1998).
2. J. P. Pouget et al., Phys. Rev. B **10**, 1801 (1974); G. Villeneuve et al., J. of Physics C: Solid State Physics **10**, 3621 (1977).
3. E. E. Chain, Appl. Opt. **30**, 2782 (1991).
4. C. N. Berglund and H. J. Guggenheim, Phys. Rev. **185**, 1022 (1969).
5. J. B. Goodenough, J. of Solid State Chemistry **3**, 490 (1971).
6. T. M. Rice, H. Launois, and J. P. Pouget, Phys. Rev. Lett. **73**, 3042 (1994); R. M. Wentzcovitch, W. W. Schulz, and P. B. Allen, Phys. Rev. Lett. **72**, 3389 (1994).
7. V. Eyert, Ann. der Physik **11**, 650 (2002).
8. K. Okazaki et al., Phys. Rev. B **69**, 165104 (2004).
9. K. Okazaki et al., Phys. Rev. B **73**, 165116 (2006).
10. E. Pavarini et al., Phys. Rev. Lett. **92**, 176403 (2004); A. Sekiyama et al., Phys. Rev. Lett. **93**, 156402 (2004).
11. S. Biermann et al., Phys. Rev. Lett. **94**, 026404 (2005); A. Liebsch, H. Ishida, and G. Bihlmayer, Phys. Rev. B **71**, 085109 (2005); M. S. Laad, L. Craco, and E. Müller-Hartmann, Phys. Rev. B **73**, 195120 (2006); M. S. Laad, L. Craco, and E. Müller-Hartmann, Europhysics Letters **69**, 984 (2005); B. Lazarovits et al., Phys. Rev. B **81**, 115117 (2010).
12. V. I. Anisimov et al., J. of Physics: Condensed Matter **9**, 7359 (1997); A. I. Lichtenstein and M. I. Katsnelson, Phys. Rev. B **57**, 6884 (1998).
13. D. B. McWhan et al., Phys. Rev. B **10**, 490 (1974).
14. O. K. Andersen, Phys. Rev. B **12**, 3060 (1975); O. K. Andersen, O. Jepsen, and M. Sob, *The Electronic Band Structure and Its Applications*, Springer-Verlag, Berlin, 1986.
15. O. K. Andersen and T. Saha-Dasgupta, Phys. Rev. B **63**, R16219 (2000).
16. W. Metzner and D. Vollhardt, Phys. Rev. Lett. **62**, 324 (1989); G. Kotliar and D. Vollhardt, Phys. Today **57**, 53 (2004); G. Kotliar et al., Rev. Mod. Phys. **78**, 865 (2006).
17. A. Georges et al., Rev. Mod. Phys. **68**, 13 (1996).
18. F. Lechermann et al., Phys. Rev. B **74**, 125120 (2006); V. I. Anisimov et al., Phys. Rev. B **71**, 125119 (2005).
19. A. I. Poteryaev et al., Phys. Rev. B **76**, 085127 (2007).
20. A. Zylbersztejn and N. F. Mott, Phys. Rev. B **11**, 4383 (1975).
21. The use of the complete data set in the fit leads to a slightly larger values for the effective magnetic moment and transition temperature for experimental and theoretical results: $p_{\rm eff}^{\rm theor} = 1.64\mu_B$, Θ^{theor} = -1980 K and $p_{\rm eff}^{\rm exp} = 1.6\mu_B$, $\Theta^{\rm exp} = -860$ K.
22. P. Werner et al., Phys. Rev. Lett. **101**, 166405 (2008).
23. A. A. Katanin et al., Phys. Rev. B **81**, 045117 (2010).
24. M. Jarrell and T. Pruschke, Zeitschrift für Physik B Condensed Matter **90**, 187 (1993).